KAPL-P-000087
(K98081)

RECEIVED
JAN 29 1999
OSTI

CONF-9806176-

InGaAsSb THERMOPHOTOVOLTAIC DIODE PHYSICS EVALUATION

G. W. Charache, P. F. Baldasaro, L. R. Danielson, D. M DePoy, M. J. Freeman,

June 1998

DISTRIBUTION OF THIS DOCUMENT IS UNLIMITED

MASTER

NOTICE

This report was prepared as an account of work sponsored by the United States Government. Neither the United States, nor the United States Department of Energy, nor any of their employees, nor any of their contractors, subcontractors, or their employees, makes any warranty, express or implied, or assumes any legal liability or responsibility for the accuracy, completeness or usefulness of any information, apparatus, product or process disclosed, or represents that its use would not infringe privately owned rights.

KAPL ATOMIC POWER LABORATORY SCHENECTADY, NEW YORK 12301

Operated for the U. S. Department of Energy
by KAPL, Inc. a Lockheed Martin company

DISCLAIMER

This report was prepared as an account of work sponsored by an agency of the United States Government. Neither the United States Government nor any agency thereof, nor any of their employees, makes any warranty, express or implied, or assumes any legal liability or responsibility for the accuracy, completeness, or usefulness of any information, apparatus, product, or process disclosed, or represents that its use would not infringe privately owned rights. Reference herein to any specific commercial product, process, or service by trade name, trademark, manufacturer, or otherwise does not necessarily constitute or imply its endorsement, recommendation, or favoring by the United States Government or any agency thereof. The views and opinions of authors expressed herein do not necessarily state or reflect those of the United States Government or any agency thereof.

DISCLAIMER

Portions of this document may be illegible in electronic image products. Images are produced from the best available original document.

InGaAsSb Thermophotovoltaic Diode Physics Evaluation

G.W. Charache, P.F. Baldasaro, L.R. Danielson, D.M. DePoy, M.J. Freeman
Lockheed-Martin, Inc., Schenectady, NY 12301-1072

C.A. Wang and H.K. Choi
Lincoln Laboratory, Massachusetts Institute of Technology, Lexington, MA 02173-9108

D.Z. Garbuzov and R.U. Martinelli
Sarnoff Corp., Princeton, NJ 08543-5300

S. Saroop, J.M. Borrego, R.J. Gutmann
Rensselaer Polytechnic Institute, Troy, NY 12180-3590

Abstract

The hotside operating temperatures for many projected thermophotovoltaic (TPV) conversion system applications are approximately 1000 $^{\circ}C$, which sets an upper limit on the TPV diode bandgap of 0.6 eV from efficiency and power density considerations. This bandgap requirement has necessitated the development of new diode material systems, never previously considered for energy generation. To date, InGaAsSb quaternary diodes grown lattice-matched on GaSb substrates have achieved the highest performance. This report relates observed diode performance to electro-optic properties such as minority carrier lifetime, diffusion length and mobility and provides initial links to microstructural properties. This analysis has bounded potential diode performance improvements. For the 0.52 eV InGaAsSb diodes used in this analysis the measured dark current is 2 x 10^{-5} A/cm^2, versus a potential Auger limit 1 x 10^{-5} A/cm^2, a radiative limit of 2 x 10^{-6} A/cm^2 (no photon recycling), and an absolute thermodynamic limit of 1.4 x 10^{-7} A/cm^2. These dark currents are equivalent to open circuit voltage gains of 20 mV (7%), 60 mV (20%) and 140 mV (45%), respectively.

The hotside operating temperatures for many projected thermophotovoltaic (TPV) conversion system applications are approximately 1000 $^{\circ}C$, which bounds the allowable TPV diode bandgap to 0.4 - 0.6 eV from efficiency and power density considerations. This bandgap requirement has necessitated the development of new diode material systems, never previously considered for energy generation application (eg. InGaAs, InPAs, InGaSb, InGaAsSb, and InAsPSb). These advances have extended and complemented the development of mid-IR detectors and lasers. To date, InGaAsSb diodes grown lattice-matched on GaSb substrates have achieved the highest performance. This report relates observed diode performance to electro-optic properties such as minority carrier lifetime, diffusion length and mobility and provides initial links to microstructural properties.

TPV diode performance is characterized by current and voltage generation. Maximizing both are critical to achieving high efficiency and power density. Current generation is quantified by quantum efficiency (ratio of electrical carriers generated to photons incident on the diode), and voltage generation is quantified by the voltage efficiency or voltage factor (ratio of open circuit voltage to diode bandgap). Both the current and voltage generation processes are controlled by minority carrier diffusion and surface recombination velocity.

Internal quantum efficiency (minority carrier collection) depends on the absorption of photons that lead to the creation of minority carriers and their diffusion to the junction interface, where minority carriers are transformed into majority carriers capable of power production. Because of the small mean free collision path of minority carriers (on the order of angstroms) the transport process can be accurately described by the first order diffusion equation as presented in various textbooks [1-3], enabling the prediction of net current into the junction and subsequently internal quantum

efficiency (QE). For a thick emitter structure typically used for InGaAsSb devices [Fig. 1], this can be approximated by:

$$QE = \frac{\alpha L_n}{\alpha^2 L_n^2 - 1}\left[\frac{\left(\frac{SL_n}{D_n} + \alpha L_n\right) - e^{-\alpha y}\left(\frac{SL_n}{D_n}\cosh\left(\frac{y}{L_n}\right) + \sinh\left(\frac{y}{L_n}\right)\right)}{\frac{SL_n}{D_n}\sinh\left(\frac{y}{L_n}\right) + \cosh\left(\frac{y}{L_n}\right)} - \alpha L_n e^{-\alpha y}\right], \qquad (1)$$

where, α is the photon absorption cross section, y is the emitter thickness, S is the front surface recombination velocity, D_n is the minority carrier diffusion coefficient, L_n is the minority carrier diffusion length ($L_n = \sqrt{D_n \cdot \tau_n}$), and τ_n is the minority carrier lifetime. Both the internal quantum efficiency and absorption coefficient are functions of photon wavelength. This approximation neglects any contribution from the depletion or base regions and is only valid for emitter thicknesses greater than 5 microns.

Open circuit voltage depends on the ratio of photo-generated current (I_l) to the internal reverse, or often termed "dark" current (I_d)

$$V_{oc} = nkT\ln\left(\frac{I_l}{I_d} + 1\right), \qquad (2)$$

where, n is the ideality factor, k is Boltzmann's constant and T is diode temperature. Dark current may be interpreted as the destruction of majority carriers that are "injected" into the minority region, (eg. when an electron is transferred from the N to the P region in Figure 1). There are several

minority carrier injection processes including thermionic emission, tunneling, and diffusion. For reasons discussed below, this analysis will focus on diffusion dominated dark current, in which case the analytic expression for a one-sided junction shown in Figure 1 is given by [1-3]:

$$I_d = q\frac{D_n}{L_n}\left(\frac{n_i^2}{N_a}\right)\left[\frac{\frac{SL_n}{D_n}\cosh\left(\frac{y}{L_n}\right)+\sinh\left(\frac{y}{L_n}\right)}{\frac{SL_n}{D_n}\sinh\left(\frac{y}{L_n}\right)+\cosh\left(\frac{y}{L_n}\right)}\right], \quad (3)$$

where n_i is the intrinsic carrier concentration and N_a is the doping level in the emitter. For a device that has a small S ($SL_n/D_n << 1$), this expression can be approximated as:

$$J_d = q\frac{D_n}{L_n}\left(\frac{n_i^2}{N_a}\right)\tanh\left(\frac{y}{L_n}\right). \quad (4)$$

As seen in Eqns. (1) and (3), the dark current (and therefore voltage efficiency from Eqn. 2) is controlled by the same electro-optic properties as the quantum efficiency, with the exception of the photon absorption cross-section. This situation contrasts quantum efficiency as minority carrier diffusion toward the diode junction with optical minority carrier generation, and voltage efficiency as minority carrier diffusion away from the junction with thermal minority carrier generation. Thus, currents with opposite direction are determined by the same parameters. By using the available TPV diode performance data, together with Eqns. 1-4 above, it is possible to bound basic electro-optic properties (diffusion length, diffusion coefficient, and lifetime) for InGaAsSb diodes.

A measure of L_n can be inferred from modeling the QE data using the relationships in Eqn.1. Figure 2 presents QE data for a high-quality p-on-n InGaAsSb homojunction with the architecture shown in Fig. 1 along with a modeled result. For this calculation, α was modeled by taking linear combinations of the various binary components [7]. The measured N-type (majority) electron mobility for the diode material in Fig. 2 is ~4000 cm^2/V-sec [4], while the P-type (minority) electron mobility is approximated as 1/2 of the majority value [5]. The minority carrier diffusion coefficient is determined from the mobility using the Einstein relationship ($D = kT\mu/q$). This yields D_n = 40-50 cm^2/s at room temperature. Using these values for α and D_n, L_n and S were varied in order to fit the measured quantum efficiency versus wavelength. This analysis indicates that emitter surface and bulk recombination effects can effectively be traded-off with each other. Assuming a negligible S, the *minimum* value of L_n and τ_n are 15 μm and 40 ns, respectively. An equally good fit to the data could be achieved with S = 4000 cm/s, L_n = 20 μm and τ_n = 90 ns.

Evaluation of dark current first requires knowledge of the source of minority carriers (i.e. thermionic emission, tunneling, or diffusion). Each source has a unique temperature dependence, revealed through the open circuit voltage sensitivity with temperature. Figures 3 shows the measured temperature sensitivity of the dark current of both InGaAs and InGaAsSb diodes. The exponential dark current dependence indicates a linear dependence of open circuit voltage, and a diffusion controlled minority carrier source. This data justifies the use of Eqns. 3 and 4 to determine an analytic estimate for dark current and open circuit voltage from the basic parameters determined above from the QE performance. Using the values of S and L_n from the quantum efficiency analysis yields a dark current density of 2×10^{-5} A/cm^2 and an open circuit voltage of 0.29-0.30 Volts at 2 A/cm^2 short circuit current (n = 1).

The calculated open circuit voltage above is lower than the measured voltage of 0.31-0.32 Volts, corroborating the basic approach presented and necessitating even longer emitter minority carrier diffusion lengths than 15 microns. In addition, the base component of the dark current, which has been neglected must also be less than $4-5\times10^{-6}$ A/cm^2, which also implies diffusion lengths in the base on the order of 1-2 microns.

The minority carrier lifetime is comprised of a number of fundamental components [6], namely,

$$\frac{1}{\tau} = \frac{1}{\tau_{SRH}} + \frac{1}{\tau_R} + \frac{1}{\tau_{AUGER}}, \qquad (5)$$

where, τ_{SRH} is the Shockley-Read-Hall (defect-limited) lifetime, τ_R is the radiative recombination lifetime and τ_{AUGER} is the Auger recombination lifetime. Shockley-Read-Hall limited lifetime is a material dependent quantity that will continue to improve as the material quality improves. Radiative lifetime is an intrinsic band-to-band direct photon emission process, and Auger is an intrinsic interband heat (phonon) generation process. Auger recombination is fundamentally the only limiting lifetime assuming photon recycling effects are taken advantage of.

The radiative lifetime is given by the reciprocal of the radiative coefficient (B) times the background carrier doping level for low-level injection conditions. The value of the B-coefficient has been determined by a number of methods, including calculations by: Garbuzov, Hall, and van Roosbroeck-Schockley [6]; as well as by experiment. Figure 4 plots the values of the B-coefficient versus bandgap using these theories as well as some limited experimental data at T = 300K. Data

points for low bandgap (< 0.6 eV) InGaAs and InGaAsSb were calculated using the van Roosbroeck-Schockley method of integrating the absorption coefficient data. As with the quantum efficiency, these calculations utilized absorption coefficients determined by linearly interpolating the binary components, similar to the method of Borrego et al. [7] using the absorption coefficient data of Palik [8]. These calculations demonstrate about an order of magnitude variation in the value of the B-coefficient for 0.5-0.55 eV material (i.e. B ~ 10^{-11} - 10^{-10} cm^3/s). For material doped 2×10^{17} cm^{-3}, this corresponds to radiative lifetimes of 70-500 ns, which is less than an order of magnitude away from the minimum lifetime extracted from quantum efficiency data.

The Auger lifetime is proportional to the inverse of the doping level squared for low level injection conditions. Values of the proportionality constant (C-coefficient) have been determined both experimentally and theoretically by a number of techniques. Figure 5 presents a literature review of these results as a function of semiconductor bandgap. Similarly to the B-coefficient data, there is a 1-2 order of magnitude spread in these values and no data available for 0.5-0.6 eV material. However, if one interpolates the lowest C-coefficient for 0.5 eV material, this yields C ~ 2×10^{-28} cm^6/s. For 2×10^{17} cm^{-3} doped material, this yields a lifetime of ~125 ns, which is within a factor of 3 of quantum efficiency predictions.

The ratio of the Auger and radiative coefficients can be estimated by measuring the electroluminescence internal quantum efficiency of InGaAsSb diodes. Neglecting the effects of SRH recombination, a simple relation exists between the internal efficiency (η_i), recombination coefficients and the emitter doping concentration (p):

$$\frac{1-\eta_i}{\eta_i} = \frac{C}{B} \cdot p \cdot \qquad (6)$$

Figure 6 plots the dependence of the internal radiative efficiency for two hole concentrations. The slope yields a reasonable fit for C/B ~ 1.55×10^{-18} cm^{-3}, which agrees well with the interpolated values from the literature, confirming the general approach presented.

Ultimately, the voltaic conversion process is limited thermodynamically through the voltage efficiency, with the maximum achievable voltage efficiency being equal to the Carnot efficiency $(T_h - T_c)/T_h$. Here, T_h is the radiator temperature and T_c is the diode temperature. The voltage limit is manifest in a minimum achievable dark current, which is set by radiative blackbody equilibrium considerations as explained in Reference 31. Diode thermal radiation emissions in effect set a limit on minority carrier radiative lifetime. From Reference 31 the thermodynamic dark current limit is given as:

$$J_d = \frac{q(N^2+1)E_g^2 kT \exp\left(-\frac{E_g}{kT}\right)}{4\pi^2 h^3 c^2} = 400(N^2+1)E_g^2 kT \exp\left(-\frac{E_g}{kT}\right) \qquad (7)$$

where, N is the index of refraction, E_g is the bandgap, h is Plank's constant, and c is the speed of light. The $(N^2 + 1)$ expression in Eqn. 7 represents radiative losses at both the front (unity term) and back (N^2 term) surfaces. It is theoretically possible to eliminate the back end radiative losses via "photon recycling" in which photons from radiative recombinations are reflected from the back surface and reabsorbed in the active diode, thereby increasing the effective carrier lifetime. The

absolute minimum theoretical dark current is then Eqn. 6 with N = 0.

Using Eqns. 5 and 7 it is possible to bound potential diode performance improvements. For the 0.52 eV InGaAsSb diodes used in this analysis the calculated dark current is 2×10^{-5} A/cm^2, versus a potential Auger limit 1×10^{-5} A/cm^2, a radiative limit of 2×10^{-6} A/cm^2 (no photon recycling), and an absolute thermodynamic limit of 1.4×10^{-7} A/cm^2. These dark currents are equivalent to open circuit voltage gains of 20 mV (7%), 60 mV (20%) and 140 mV (45%) respectively. Fig. 7 illustrates the comparison of the diffusion-limited dark current (Eqn. 4), the radiative limited dark current (Eqn. 7), a potential Auger-limited dark current and some experimental data for InGaAsSb devices.

In order to further characterize the limiting recombination mechanisms, minority carrier lifetime measurements were performed. Double-capped heterojunctions of various thicknesses have been utilized to directly measure bulk lifetime and surface recombination velocity [32]. This has yielded a minimum value of bulk lifetime of 100 ns and a surface recombination velocity of 3600 cm/s. For these measurements as the laser intensity is reduced, the measured lifetime increases which eliminates defects as the dominant lifetime mechanism. Both the minimum bulk lifetime and surface recombination values are higher than the initial estimates from the quantum efficiency and dark current data; while the minimum lifetime is comparable to the estimated Auger limit. This establishes that equal probabilities exist of minority carrier recombination occurring within the bulk or at the surface.

The above analyses are oversimplified in that they assume homogeneous diode material, uniform doping, uniform electro-optic, abrupt interfaces, etc. However, it is well established that III-V

semiconductor alloys are not homogeneous and are subject to ordering, composition modulation and phase separation [33-35]. Although several processes have been identified that may currently limit minority carrier lifetime, a number of anomalous phenomena have indicated that the detailed InGaAsSb microstructure may influence the bulk lifetime limiting processes, including:

- The voltage efficiency of InGaAsSb alloys has remained essentially constant as the bandgap has decreased from 0.55 to 0.51 eV. This indicates that material quality (i.e. minority carrier lifetime) is increasing as the miscibility gap is approached.
- Diffuse streaking indicative of compositional modulation is observed in TEM diffraction patterns on all samples; even in the highest performing OMVPE-grown TPV diodes. This implies that the material structure is at a minimum influencing the electro-optical characteristics of the device [33].
- Higher quantum efficiency has been observed for devices grown on <100> misoriented 2° -<110>, even though the surface morphology is not as good as that observed on <100> misoriented 6° -<111B>

These phenomena may be tentatively explained by spontaneous lateral composition modulation in InGaAsSb alloys [32-34]. The observed composition modulation causes localized changes in the bandstructure that form type-II heterojunctions between the various domains [36]. This domain formation, oriented perpendicular to the growth plane, spatially isolate electrons and holes that lead to increased carrier lifetimes. In addition, these domains will be under high levels of strain relative to each other due to the tendency to phase separate into GaAs and InSb-rich phases. This again causes changes in the local bandstructure that may suppress Auger recombination. In

essence a "natural" superlattice has been created analogous to the artificially structured materials used in laser diodes for the suppression of Auger recombination. The rough surface morphology in the "best" devices may be another manifestation of this composition modulation.

The developmental nature of InGaAsSb diode materials and the analysis presented above suggests that bulk defects are not limiting the minority carrier lifetime at this time. However, a detailed survey and analysis of surface, bulk-Auger and bulk-radiative processes in low bandgap III-V systems is needed in order to reduce the uncertainty in the B- and C-coefficients (along with their dependence on microstructural properties). Little experimental data on low bandgap materials of interest has been found to date, and extrapolations based on the limited available data shows at least an order of magnitude variation. It is clear that the InGaAsSb material system has high performance potential, however, it is not clear which of the available III-V materials options have the highest theoretical performance as reflected in the effects of microstructure inhomogeneity on the limiting lifetime processes.

With further minimization of surface recombination and the establishment of bulk-radiative limited voltage and current generation, it may be possible to further improve performance with the alternative diode architecture presented in Figure 8. This "2-pass" architecture has three potential advantages: 1) above-bandgap photons are reflected at the back surface, maximizing the absorption of near-bandgap photons which typically have lower absorption cross sections, 2) it minimizes the emitter thickness which reduces integral minority carrier recombination and increases voltage, and 3) increases below bandgap reflection in the vicinity of the bandgap energy which increases spectral efficiency.

References

[1] A. Fahenbrush and R. Bube, Fundamentals of Solar Cells (Academic Press, New York, 1983).

[2] M.A. Green, High Efficiency Solar Cells,

[3] H.J. Hovel, "Solar Cells" in Semiconductors and Semimetals, vol. 2 (Academic Press, New York 1975).

[4] C.A. Wang, H.K. Choi, G.W. Turner, D.L. Spears, M.J. Manfra, and G.W. Charache, AIP Conf. Proc., **401**, 75 (1997).

[5] M. Lovejoy and M. Lundstrom, "Temperature Dependent Minority and Majority Carriers in Degenerately-Doped GaAs," Appl. Phys. Lett., **67**, 21 (1995).

[6] R.K. Ahrenkiel, "Minority Carrier Lifetime in III-V Semiconductors" in Semiconductors and Semimetals, vol. 39 (Academic Press, New York 1993).

[7] J. Borrego, M. Zierak and G. Charache, AIP Conf. Proc., **321**, 371 (1995).

[8] E.D. Palik Ed., Handbook of Optical Constants of Solids Vol. I and II (Academic Press, New York, 1985, 1991).

[9] M. Levinshtein, S. Rumyantsev, and M. Shur Eds., Handbook Series on Semiconductor Parameters Vol. I, (World Scientific, New York, 1996).

[10] S. Adachi, Ed., Properties of Indium Phosphide, (INSPEC, New York, 1991).

[11] C.H. Henry, R.A. Logan, F.R. Merrit and C.G. Betha, Electron Lett, **20**, 358 (1984).

[12] E. Winter and E.P. Ippen, Appl. Phys. Lett., **44**, 999 (1984).

[13] M. Osinski, P.G. Eliseev, V.A. Smagley, P. Uppal and K. Ritter, Proc. Sensors and Electron. Dev. Sym., 7 (1997).

[14] P. Jenkins, G. Landis, I. Weinberg and K. Kneisel, 22nd IEEE PVSC, 177 (1991)

[15] T. Uji, K. Iwamoto and R. Lang, Trans. Electon Dev., **30**, 316 (1983).

[16] W. Bardyszewski and D. Yevick, Jl. Appl. Phys., **58**, 2713 (1985).

[17] G. Benz and R. Conradt, Phys. Rev B, **16**, 843 (1977).

[18] P.T. Landsberg, Solid State Electron., **30**, 1107 (1987).

[19] M. Takeshima, Jap. Jl. Appl. Phys., **22**, 491 (1983).

[20] B.L. Gel'mont and Z.N. Sokolova, Sov. Phys. Semicond., **16**, 1067 (1982).

[21] D. Yevick and W. Barduszwski, Appl. Phys. Lett., **51**, 124 (1987).

[22] A.N. Titkov, G.N. Iluridze, I.F. Mironov, and V.A. Cheban, Sov. Phys. Semicond., **20**, 14, (1986).

[23] G.P. Agrawal and N.K. Dutta, Long Wavelength Semiconductor Lasers (Van Nostrand Reinlhold, New York, 1985)

[24] A. Sagimura, Jl. Appl. Phys., **51**, 4405 (1980).

[25] C.B. Su, R. Olshansky, W. Powazinik, and J. Manning, Trans. Electon. Dev., **30**, 1594 (1983).

[26] G.N. Iluridze, I.F. Mironov, A.N. Titkov and V.A. Cheban, Sov. Phys. Semicond., **20**, 310, (1986).

[27] A. Haug, Appl. Phys. A, **51**, 354 (1990).

[28] N.K. Dutta and R.J. Nelson, Jl. Appl. Phys. **53**, 74 (1982).

[29] S. Hausser, G. Fuchs, A. Hangleiter, K. Streubel, W.T. Tsang, Appl. Phys. Lett., **56**, 913 (1990).

[30] M.E. Prise, Appl. Phys. Lett, **45**, 652 (1984).

[31] C. Henry, Jl. Appl. Phys., **51**, 4494 (1980).

[32] S. Saroop, presented at the 40th Electronic Materials Conference, Charlottesville, VA (1998).

[33] Y.C. Chen, V. Bucklen, M. Freeman, R.P. Cardines Jr., and K. Raian, presented at the 40th Electronic Materials Conference, Charlottesville, VA (1998).

[34] A. Zunger and S. Mahajan, "Atomic Ordering and Phase Separation in Epitaxial III-V Alloys," in Handbook of Semiconductors, vol. 3, edited by T.S. Moss (Elsevier Science B.V., Amsterdam, 1994).

[35] J.M. Millunchick, T.D. Twensten, S.R. Lee, D.M. Follstaedt, E.D. Jones, S.P. Ahrenkiel, Y. Zhang, H.M. Cheong, and A. Mascarenhas, MRS Bulletin, July 1997 pp. 38-43.

[36] R.K. Ahrenkiel, S.P. Ahrenkiel, D.J. Arent, and J.M. Olsen, Appl Phys. Lett., 70(6), 756 (1997).

List of Figures

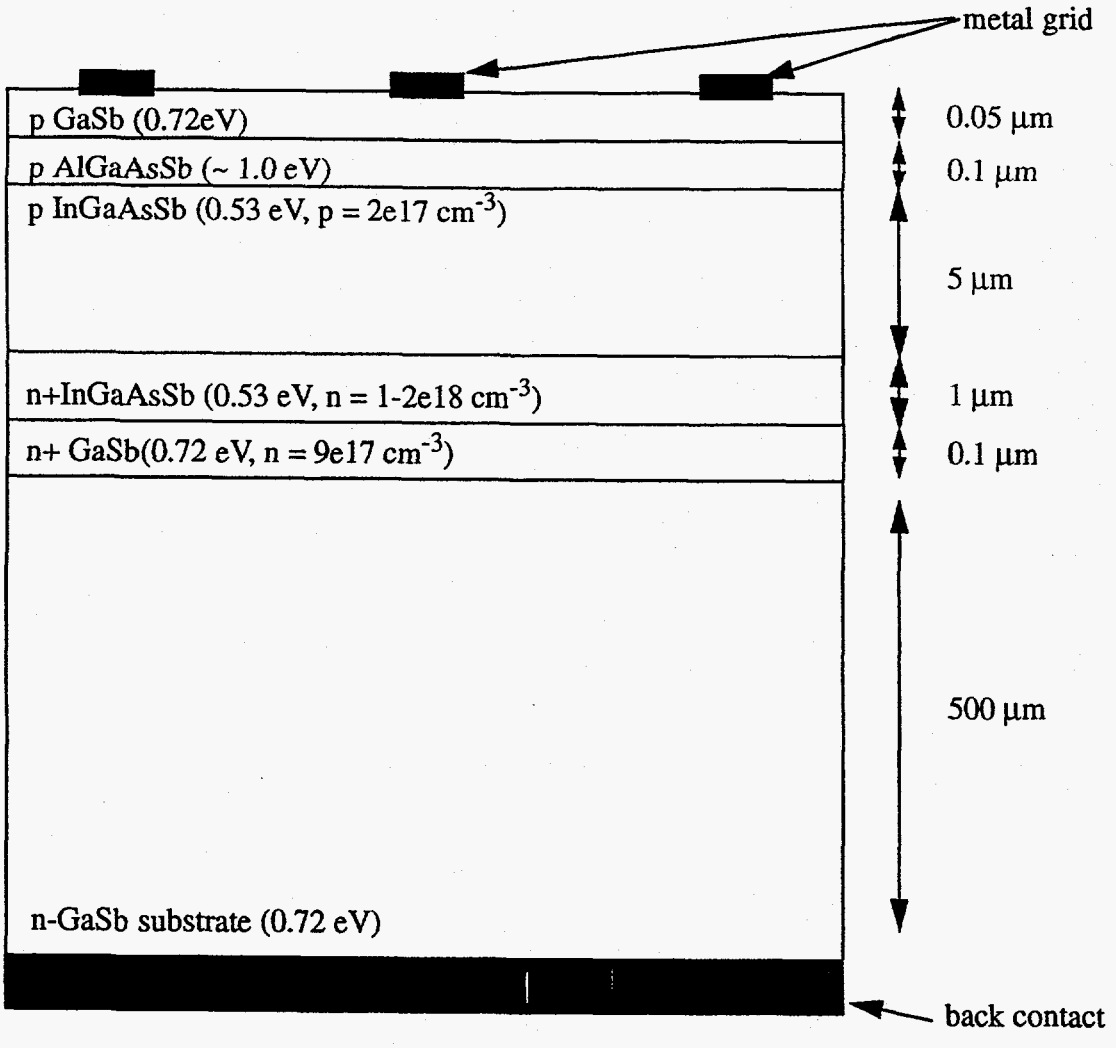
metal grid
p GaSb (0.72eV)
p AlGaAsSb (~ 1.0 eV)
p InGaAsSb (0.53 eV, p = 2e17 cm-3)
n+InGaAsSb (0.53 eV, n = 1-2e18 cm-3)
n+ GaSb(0.72 eV, n = 9e17 cm-3)
n-GaSb substrate (0.72 eV)
0.05 μm
0.1 μm
5 μm
1 μm
0.1 μm
500 μm
back contact

Figure 1

REPRODUCED AT GOVT EXPENSE #48

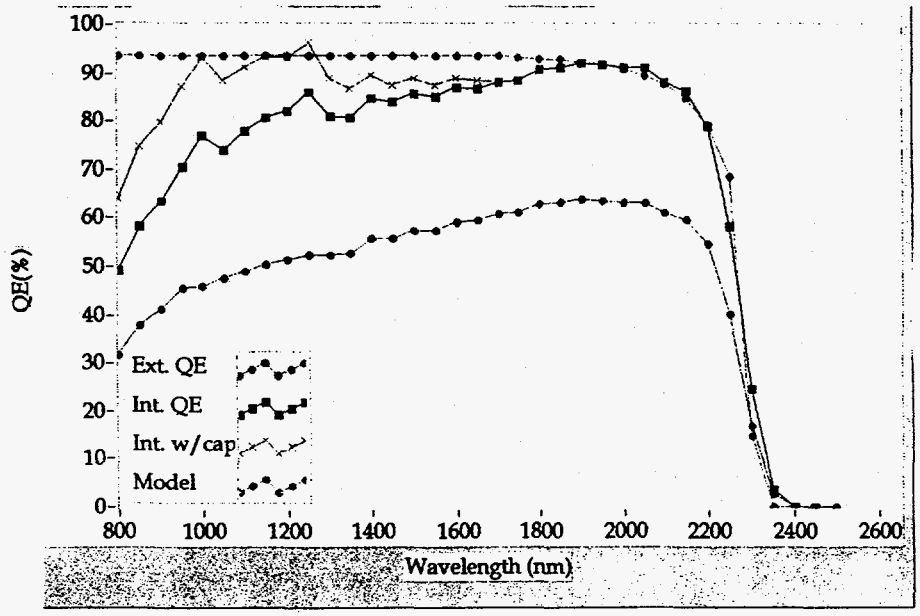

Figure 2

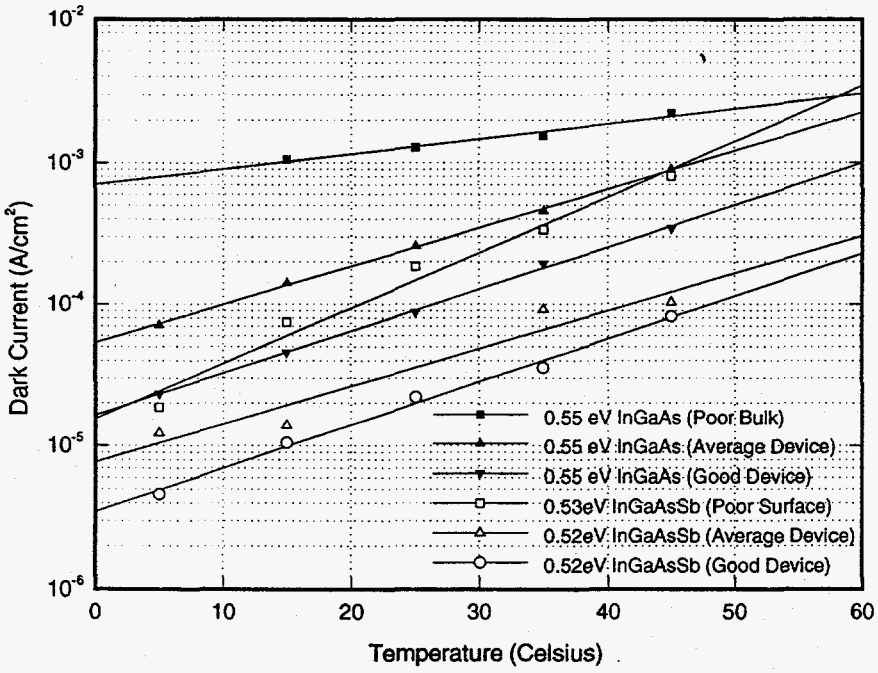
Dark Current (A/cm²)
10⁻²
10⁻³
10⁻⁴
10⁻⁵
10⁻⁶
0
10
20
30
40
50
60
Temperature (Celsius)
0.55 eV InGaAs (Poor Bulk)
0.55 eV InGaAs (Average Device)
0.55 eV InGaAs (Good Device)
0.53eV InGaAsSb (Poor Surface)
0.52eV InGaAsSb (Average Device)
0.52eV InGaAsSb (Good Device)

Figure 3

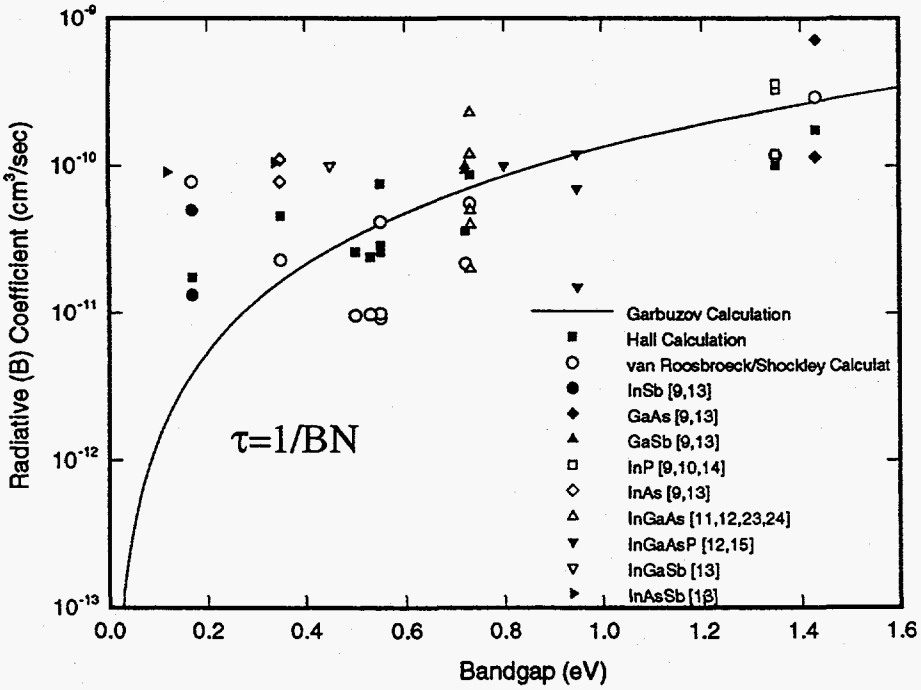
Radiative (B) Coefficient (cm³/sec)
10⁻⁹
10⁻¹⁰
10⁻¹¹
10⁻¹²
10⁻¹³
0.0
0.2
0.4
0.6
0.8
1.0
1.2
1.4
1.6
Bandgap (eV)
τ=1/BN
Garbuzov Calculation
Hall Calculation
van Roosbroeck/Shockley Calculat
InSb [9,13]
GaAs [9,13]
GaSb [9,13]
InP [9,10,14]
InAs [9,13]
InGaAs [11,12,23,24]
InGaAsP [12,15]
InGaSb [13]
InAsSb [13]

Figure 4

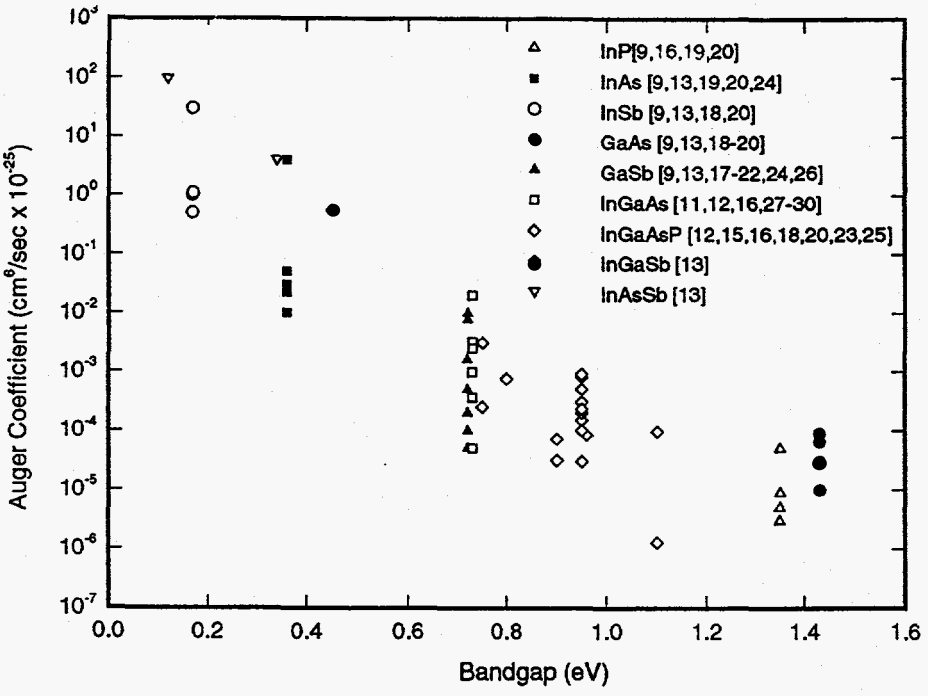
Auger Coefficient (cm⁶/sec x 10⁻²⁵)
Bandgap (eV)
InP[9,16,19,20]
InAs [9,13,19,20,24]
InSb [9,13,18,20]
GaAs [9,13,18-20]
GaSb [9,13,17-22,24,26]
InGaAs [11,12,16,27-30]
InGaAsP [12,15,16,18,20,23,25]
InGaSb [13]
InAsSb [13]

Figure 5

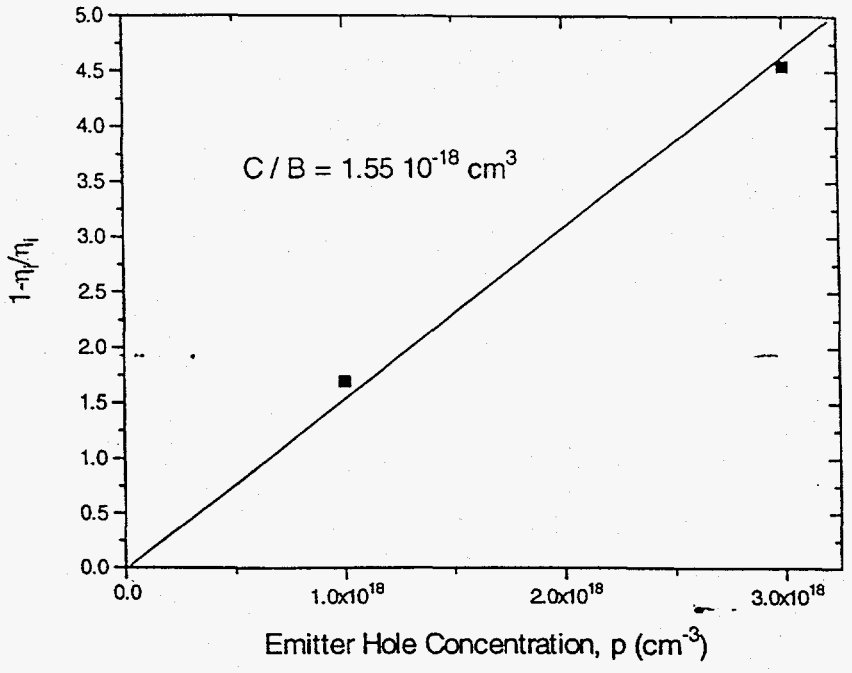
5.0
4.5
4.0
3.5
3.0
2.5
2.0
1.5
1.0
0.5
0.0
1-η_i/η_i
C / B = 1.55 10^-18 cm^3
0.0
1.0x10^18
2.0x10^18
3.0x10^18
Emitter Hole Concentration, p (cm^-3)

Figure 6

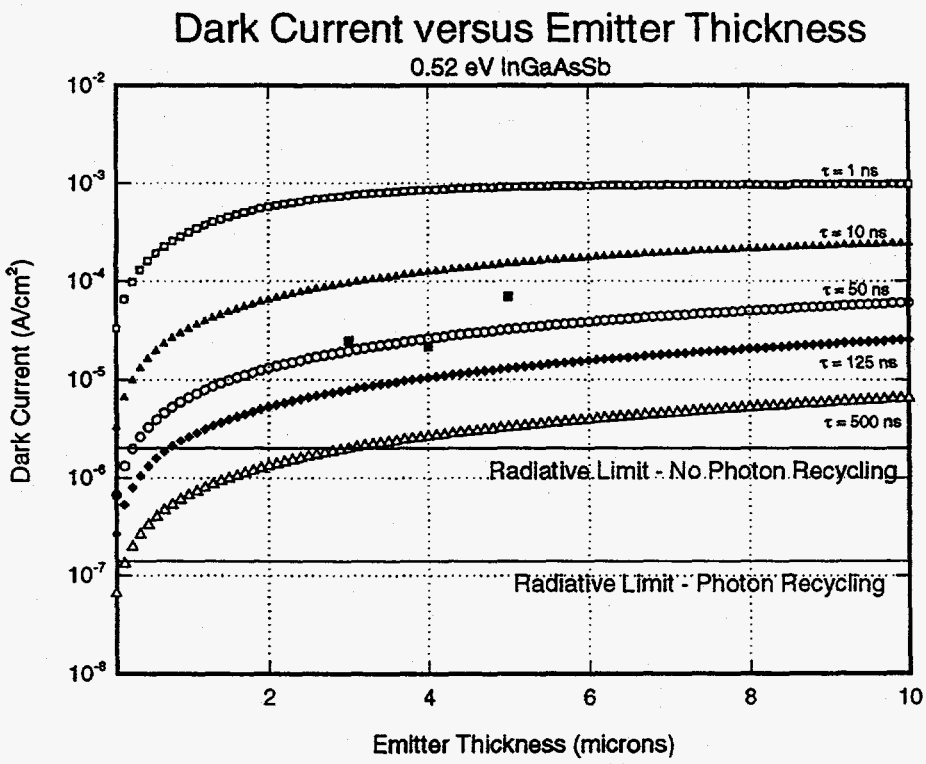
Dark Current versus Emitter Thickness
0.52 eV InGaAsSb
Dark Current (A/cm²)
Emitter Thickness (microns)
τ = 1 ns
τ = 10 ns
τ = 50 ns
τ = 125 ns
τ = 500 ns
Radiative Limit - No Photon Recycling
Radiative Limit - Photon Recycling

Figure 7

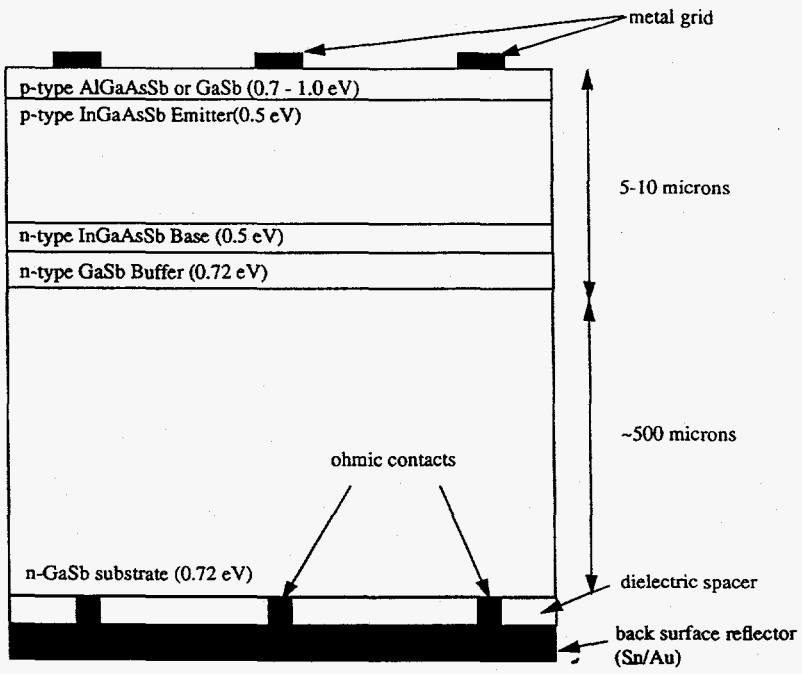
metal grid
p-type AlGaAsSb or GaSb (0.7 - 1.0 eV)
p-type InGaAsSb Emitter(0.5 eV)
5-10 microns
n-type InGaAsSb Base (0.5 eV)
n-type GaSb Buffer (0.72 eV)
~500 microns
ohmic contacts
n-GaSb substrate (0.72 eV)
dielectric spacer
back surface reflector
(Sn/Au)

Figure 8